

Final Technical Report

Parametric Investigation of Droplet Atomization and Dispersion of Liquid Fire Suppressants

Project Identifier: 5A/1/02

Date: December 30, 2003

The views and conclusions contained in this document are those of the authors and should not be interpreted as representing the official policies, either expressed or implied, of the Strategic Environmental Research and Development Program, (enter the name of the reporting agency), or any other part of the U.S. Government.

*Sponsored by:
The Department of Defense
Strategic Environmental Research and Development Program*

SUMMARY:**Task Objectives:**

The objective of this project was to develop a startup data set to guide the modeling efforts under the project "Fire Suppressant Dynamics in Cluttered DoD Weapon System Compartments (NGP 6A/1)," and to develop a parametric data set for model validation.

Benefit:

Established correlation of the agent/spray properties, agent atomization methods, and agent dispersion effectiveness that will enable (in fire modeling and scale-up to intermediate- and full-scale testing, such as in NGP project 6A/1) optimizing the fire suppression performance of misted liquid systems.

Technical Problems:

The collaborative effort worked well, in which our experiments were coordinated by the fruitful and frequent discussions with the NGP 6A/1 participants (Sandia Nat'l Labs, NavAir, and the USAF 46th Test Wing), and resulted in a data set that was responsive to the modeling needs. Hence, there were no modifications of objectives or technical problems.

General Methodology:

Investigate at laboratory-scale, engine nacelle-like conditions, the atomization and dispersion of different liquid agents within an enclosure, with and without obstructions, and evaluate the effectiveness of the agent to reach the location of a fire. Investigate experimentally the effect of agent composition and physical properties, spray characteristics (e.g., droplet size/velocity distribution, spray pattern), agent atomizer design (deployment speed and direction), and obstacle shape, size, position relative to the agent deployment device, and temperature on agent atomization and dispersion under nonburning conditions. The laboratory-scale experiments were carried out in the NIST Spray Combustion Test bed. Droplet dispersion was characterized qualitatively by high-speed video, and laser sheet illumination techniques. Quantitative size and velocity measurements of the dispersed phase were carried out using phase Doppler interferometry and particle image velocimetry. The investigation was coordinated with the efforts of NGP project 6A/1 to define the required experimental configuration, operating conditions, and measurement data needs for their aircraft engine nacelle fire simulations.

In FY2000, discussions with the project team of NGP 6A/1 defined the baseline case, namely, the experimental configuration, operating conditions, and experimental data needs required to assist the computational modeling effort. A startup data set was obtained that defined the required inlet and boundary conditions for the NGP 6A/1 computational work. In FY2001, efforts were directed to obtain a full parametric data set. In FY2002, tasks were defined with the project team of NGP 6A/1, which included modifications to the experimental configuration, operating conditions, and specification of experimental data not provided in FY2000 and FY2001, and was required to assist the computational submodel development effort.

Technical Results:

Air velocities were measured to characterize the homogeneous turbulent aerodynamic flow field, and droplet sizes and velocities were obtained upstream and downstream of selected obstacles (i.e., body centered cube of spheres, and a cylinder under heated and unheated conditions). Liquids with a range of boiling points (i.e., water, HFE-7100, and HFE-7000) were used to characterize the effect of liquid vaporization on droplet transport. Particle image velocimetry (PIV), phase Doppler interferometry, and laser sheet photography were the employed measurement diagnostics.

Particle image velocimetry measurements and preliminary numerical predictions using the Vulcan fire code were completed to examine the flow field dynamics of highly turbulent homogeneous flow over obstacles, and droplet transport in such flow fields. Comparison of numerical predictions to PIV measurements showed good qualitative agreement in spatial distribution of the mean and RMS velocities with a 20 % overprediction in mean streamwise velocity and 15 % underprediction in the RMS values. A numerical sensitivity study using HFE-7100 revealed a strong dependency of droplet transport on initial droplet size for the flow range and droplet sizes that are of interest in practical agent delivery systems.

Particle image velocimetry measurements were carried out in the droplet-laden, homogeneous turbulent flow over both an unheated and heated cylinder, and body-centered cube (BCC) arrangement of spheres. Transport of both water droplets and aerosol particles was characterized upstream and downstream of these obstacles. Data were recorded for the cylinder at ambient temperature and after being heated to 423 K to estimate the effects of the hot cylinder surface on droplet transport. The results indicated that smaller droplets were entrained into the recirculation region behind the cylinder while the larger droplets impacted the cylinder surface, accumulated and dripped off, and/or rebounded off the surface and dispersed radially outward into the free stream. The Weber number was too low to lead to droplet shattering. Significant cooling of the cylinder surface from the initial preset temperature, which resulted from spray impingement, was observed for the heated cylinder, in addition to the presence of a vapor stream downstream of the cylinder along the shear layer region between the recirculation zone and free stream. For the BCC (with a blockage ratio of about 64 %), both droplets (having a wide size distribution) and seed particles (generated from a fogging device, and representing smaller size droplets of around 1 μm) were transported around and through the BCC, with significantly more liquid accumulation and dripping than for the cylinder. Comparison of the velocity fields obtained with water droplets from a pressure-jet atomizer and the 1 mm size aerosol particles indicated that dispersion of droplets/particles around an obstacle is dependent on its size.

Phase Doppler interferometry measurements were carried out to obtain droplet size and velocity distributions in a droplet-laden homogeneous turbulent flow field around the cylindrical obstacle. Results indicated that most impinging droplets coat the surface with few droplets rebounding back into the free stream. Rebounding droplets were generally less than 30 μm , corresponding to the higher probability portion of the size distribution. Downstream in the wake region of the cylinder, a distribution of smaller size droplets (generally, of less than 30 μm)

was entrained in the recirculation zone. Near the heated cylinder surface, droplet vaporization results in smaller mean droplet sizes, as compared to the ambient case. Droplet sizes and velocities that were obtained for water, HFE-7100 (with a boiling point of 334 K), and HFE-7000 (with a boiling point of 307 K), were compared for the unheated cylinder case. It was observed during these experiments that both HFE-7000 and HFE-7100 vaporized more readily than water (presumably due to their lower boiling points), without any dripping of liquid off of the cylinder surface, and that their size distributions resulted in means droplet sizes smaller than that for water.

Important Findings and Conclusions:

- Droplet transport of liquid suppressants past an obstacle.
 - Transport of liquid droplets downstream on the cylinder was dependent on the droplet size. Droplets larger than 30 μm - 50 μm tend to impinge on the cylinder surface or disperse around the cylinder to be transported far downstream of the obstacle. Droplets smaller than 30 μm - 50 μm entrain into the gas stream and transport around the cylinder into the recirculation region behind the obstacle.
 - Droplets with lower boiling points tend to vaporize more readily, resulting in vaporization of most droplets before reaching the obstacle.
 - With a blockage ratio of ~64 %, less than 5 % of the total liquid dripped off the body-centered cube, thus most of the liquid suppressant will pass through complex obstacles unless the blockage ratio is much higher.
- Effects of cylinder preheating on the transport of liquid agent in the vicinity of the obstacle.
 - Liquid dripping off the cylindrical surface was eliminated from the hot surface due to vaporization of the liquid. The surface was heated to 423 K.
 - A vapor stream formed in the shear layer downstream of the cylinder due to liquid vaporizing off of the hot surface.
 - Coating of the obstacle surface with droplets resulted in significant surface cooling, which can be advantageous in preventing re-ignition.
 - Droplet mean size decreased and velocity decreased with increased cylinder temperature.
- Boiling point effects on the transport of liquid agents.
 - Liquid impingement, coating, and dripping were eliminated for the lower boiling point agents (i.e., HFE-7000 with a boiling point of 307 K and HFE-7100 with a boiling point of 334 K) due to rapid vaporization.
 - Droplet mean size decreased and velocity increased with lower boiling point agents.

- Input experimental data set for development of the spray/surface interaction model in the Sandia Vulcan fire code.
 - It is improbable that shattering will occur for the Weber numbers (i.e., droplet sizes and velocities) encountered for the given operating conditions (typical of that in an engine nacelle), thus it need not be considered in the spray model.
 - Initial conditions provided for droplet size and velocity were used to obtain good agreement with a preliminary simulation carried out with the Vulcan fire code. As the code is further developed, the remainder of the data set (including data for different agents, and for an unheated and heated cylinder) will be useful for code validation.

Significant Hardware Development:

Development of an enclosed Plexiglas spray chamber that can be used to investigate spray transport phenomena over unheated and heated obstructions. The system can provide experimental data for input and validation of fire models that simulate spray-clutter interactive environments.

Special Comments:

Several points should be considered during future research, as listed below:

- Coating of an obstacle surface by a liquid agent may be considered as a positive event in that the agent will cool the surface and inhibit reignition events.
- It takes a very high blockage ratio to have a significant influence on the transport of agent past the obstacle and prevent the transport of agent to a flame.
- Assuming a positive correlation between droplet size and velocity, larger droplets move ballistically and smaller droplets will be entrained into the surrounding aerodynamic flow field. Thus, different strategies to control and optimize the spatial dispersion of droplets can be developed by including a wide range of droplet sizes (e.g., to disperse droplets far downstream of the atomizer and/or immediately behind a close obstacle). The atomizer design must also be considered since it dictates the initial spatial dispersion of droplets.
- Strategies can be developed to exploit the effect of different agent physical properties, e.g., boiling point, on droplet vaporization and transport. One can envision multicomponent (miscible mixtures) and multiphase (with solid particle inclusions like potassium carbonate) droplets. Thus, these droplets can be engineered ('designer droplets') so that preferential vaporization of the carrier liquid occurs while the active agent is successfully introduced to the flame.

These points may be important for consideration in the development of fire suppression models and validated simulations.

Implications for Further Research:

Of paramount importance for validation of computational models is to provide a database with specified experimental uncertainties so that the modeler will have the highest confidence in using the data. To achieve such a database requires inlet and boundary conditions, and experimental measurements to be repeated several times to determine experimental uncertainty levels. In addition, as the Vulcan fire code continues to be developed, data will be required to address specific issues that arise regarding the actual physics. This study presented some information on the effect of agent boiling point; however, it would be more efficacious to carry out a parametric investigation of different agent physical properties on droplet transport processes. Additional parameters such as atomizer design, spray pattern, droplet spatial variation containing specified droplet sizes, more complicated obstacle arrangements, and droplet composition (e.g., droplets with other effective suppressants such as in miscible solution or colloidal suspensions) may provide important information for the modeling effort. Also, investigating different scenarios of fire suppression by putting tail tale heaters behind obstacles and introducing the liquid agent suppressant is important to confirm the effect of various spray characteristics like droplet size, velocity, composition, and spatial density, on transport and extinguishment of a fire.

BIBLIOGRAPHY OF PAPERS:

1. Presser, C., Widmann, J.F., DesJardin, P.E., and Gritzo, L.A., "Measurements and Numerical Predictions of Liquid Agent Dispersal Around Solid Obstacles," Proc. Halon Options Technical Working Conf. (HOTWC-2001), pp. 122-130, New Mexico Engineering Research Institute, Albuquerque, NM, 2001.
2. Presser, C., Widmann, J.F., DesJardin, P.E., and Gritzo, L.A. "Measurement and Numerical Prediction of Homogeneous Turbulent Flow over a Cylinder: A Baseline for Droplet-Laden Flow Studies," AIAA 2002-0905, Am. Inst. Aero. Astro., Washington, DC, 2002.
3. Presser, C., Widmann, J.F., and Papadopoulos, G., "Liquid Agent Transport Around Solid Obstacles," Proc. 12th Halon Options Technical Working Conf. (HOTWC-2002), NIST Special Publication 984 (R.G. Gann and P.A. Reneke, Eds.), on CD, NIST, Gaithersburg, MD, 2002.
4. DesJardin, P.E., Presser, C., Disimile, P.J., and Tucker, J.R., "A Droplet Impact Model for Agent Transport in Engine Nacelles," Proc. 12th Halon Options Technical Working Conf. (HOTWC-2002), NIST Special Publication 984 (R.G. Gann and P.A. Reneke, Eds.), on CD, NIST, Gaithersburg, MD, 2002.
5. Presser, C., Widmann, J.F., and Papadopoulos, G., "PIV Measurements of Droplet Transport in a Homogeneous Turbulent Flow over a Cylinder," AIAA 2003-0846, Am. Inst. Aero. Astro., Washington, DC, 2003.

6. DesJardin, P.E., Presser, C., Disimile, P.J., and Tucker, J.R., "A Phenomenological Droplet Impact Model for Lagrangian Spray Transport." AIAA 2003-1322, Am. Inst. Aero. Astro., Washington, DC, 2003.
7. Presser, C., Avedisian, C.T., and Johnson, B.S., "Phase Doppler Measurements of Liquid Agent Transport over a Heated Cylinder," Proc. 13th Halon Options Technical Working Conf. (HOTWC-2003), NIST Special Publication 984-1 (R.G. Gann, S.R. Burgess, and P.A. Reneke, Eds.), on CD, NIST, Gaithersburg, MD, 2003.
8. Presser, C., Papadopoulos, G., and Widmann, J.F., "PIV Measurements in a Droplet-Laden Homogeneous Turbulent Flow over a Cylinder," Proc. 16th Annual Conf. on Liquid Atomization and Spray Systems (ILASS Americas '03), on CD, Monterey, CA, 2003.
9. Presser, C., Papadopoulos, G., and Widmann, J.F., "Droplet-Laden Homogeneous Turbulent Flow Past Unheated and Heated Cylinders," Proc. ASME/JSME Joint Fluids Engineering Conf. (FEDSM'03), FEDSM2003-45240 (on CD), Am. Soc. Mech. Eng., New York, NY, 2003.
10. Presser, C., Avedisian, C.T., and Johnson, B.S., "Phase Doppler Measurements of Liquid Fire Suppressants over a Heated Cylinder," AIAA 2004-0479, Am. Inst. Aero. Astro., Washington, DC, 2004.
11. Presser C., and Avedisian C.T., "Transport of High Boiling-Point Fire Suppressants in a Droplet-Laden Homogeneous Turbulent Flow past a Heated Cylinder," submitted to the International Symposium on Combustions (2004).

DETAILED PROJECT DESCRIPTION:

Gas-Phase Velocity around Three Cylindrical Obstructions in a Homogenous Turbulent Flow Field

Under the modeling effort in project NGP 6A/1, Sandia National Laboratories required experimental particle-laden, homogeneous turbulence data of the fluid flow upstream and wake region downstream of obstacles. These data would be used to develop and validate the sub-grid turbulence model that is used in the Sandia VULCAN fire code. Information of interest included the gas mean and turbulence velocities, as well as droplet characteristics, at the inlet and in the region upstream and downstream of the obstruction. Of concern was to provide an experimental arrangement with boundary conditions that was devoid of any regions of gas recirculation. Measurements were carried out under operating conditions similar to that found in an aircraft engine nacelle.

The initial experimental arrangement, shown in Fig. 1, included an octagon-shaped Plexiglas insert (with a wall thickness of 6 mm, length of 610 mm, and minor and major axes of 560 mm and 760 mm, respectively) that served as a boundary condition. An octagon shape was used to accommodate the measurement requirements for the planar imaging velocimetry (that provided gas-phase turbulence intensity) and phase Doppler interferometry (that

measured agent droplet size and velocity) optical arrangements. A seeding system was used to introduce seed particles as a marker for the optical diagnostics and for flow visualization. The octagon shape did not impose any difficulties for the Sandia model. A honeycomb layer (51 mm thick with 3 mm size cells) was used to straighten the airflow, which was co-positioned around an injector for introducing liquid agent. Grid-generated turbulence was imposed on the air stream by placing a layer of wire mesh screen (with 13 mm size cells) downstream of the honeycomb. The obstacle was a tube that was placed across the turbulent flow field downstream of the wire mesh screen. Honeycomb and wire mesh with different cell sizes, were used to generate a baseline integral length scale. For these experiments, the incoming air (supplied from a 94.4 L/s compressor) was directed entirely through a selected 125 mm by 254 mm rectangular cross-sectional portion of the honeycomb and then through wire mesh screen (placed 25 mm downstream of the honeycomb), as shown in Fig. 1. The integral and Kolmogorov length scales of turbulence were estimated to be 3 cm and 100 μm , respectively. Three obstacle tubes with diameters of 3 mm, 13 mm, and 32 mm, were chosen to span ranges of clutter sizes smaller, on the same order, and larger than the integral length scales of turbulence. The obstacles were placed 100 mm downstream of the honeycomb and grid, as will be discussed in more detail. A stepper-motor-driven traversing system translated the entire assembly, and permitted measurements of the flow field properties at selected locations downstream of the injector.

The 3-dimensional velocity flow field was characterized using a PIV system from Dantec Dynamics, Inc.* Particle image velocimetry is a non-intrusive field measuring technique (as opposed to a single-point diagnostic method) that can measure two or three components of velocity. The PIV images were obtained in a plane corresponding to a laser light sheet that was oriented downward from above the Plexiglas chamber and onto a cross section of the obstacle. The method required seed particles to be added to the flow, which were generated by a pencil fogger and were 1 mm in diameter. The seed particles were assumed to follow the streamlines and act as tracers. A separate supply of air (negligible with regard to the total compressor air flow supplied to the experiment) was used to carry the fog aerosol into the main air stream downstream of the distributor plate. The time between the images was determined by the time between laser pulses. The spatial displacement of the seed particles, corresponding to two images separated by a known time period (the time between laser pulses was 70 μs), was measured and the velocity was deduced. The spatial resolution of the measurements depends directly upon the pixel resolution, field of view, and laser light sheet thickness, and indirectly on the seeding density. For the measurements presented here, the spatial resolution was approximately 600 μm . The 3-D stereo PIV system differed from traditional PIV systems in that two charged-couple device (CCD) cameras were used, and three velocity components were measured.

A 50 mJ Nd:YAG laser was used as the illumination source for the PIV measurements. The pulse duration of the laser light sheet was about 5 ns, and the wavelength of the light was 532 nm. A pair of 12-bit double-frame CCD

* Certain commercial equipment or materials are identified in this publication to specify adequately the experimental procedure. Such identification does not imply recommendation or endorsement by the National Institute of Standards and Technology, nor does it imply that the materials or equipment are necessarily the best available for this purpose.

cameras with a resolution of 1024 x 1280 pixels was used to obtain the images. Special camera mounts were utilized to permit the rotation of the camera body with respect to the camera lens so the Scheimpflug condition was satisfied, permitting the laser sheet to be in focus despite the non-orthogonal camera alignment. Bandpass filters (center wavelength = 532 nm, acceptance window = 30 nm) were used to reject the broadband white light from the room. The two cameras were placed at angles of about 70° and 110°, as measured from the forward direction of propagation of the laser pulse. The processed results were presented as a composite mapping of individual planar regions that were about 40 mm in height and 50 mm in width. Statistics were obtained from about 500 - 700 individual records. Each field of view represents about 9000 vectors. Measurements of the flow field were carried out along the centerline of the measurement area, and at two planes, ± 25 mm from the centerline location.

The results indicated a mean flow velocity of 4.5 m/s, corresponding to a Reynolds number of 3700 (based on the grid cell size), and provided a homogenous distribution of turbulence across the measurement area. This flow velocity was also representative of airflow speeds through aircraft engine nacelles. Particle image velocimetry was used to obtain instantaneous two-dimensional images of the air velocity (i.e., three components of velocity). These images were then used to construct the streamwise (W) and two cross-stream (U and V) mean and root mean square (RMS) profiles, both upstream and downstream of the cylinder, and along the centerline location. Downstream of the honeycomb, the baseline flow field was found to be relatively uniform throughout the measurement field, as shown in Figs. 2 and 3 (gas streamwise component of velocity, $v_w \cong 4.5$ m/s, and turbulence intensity, $\tau_w \cong 13$ %), except immediately downstream of the honeycomb. The local jetting downstream of the honeycomb exit was found to decay with increasing streamwise distance, and became negligible after 25 mm. Based on this observation, the wire grid mesh that was used to generate turbulence was placed at this location. The flow downstream of the wire mesh was obtained along the centerline of the measurement region.

Nonuniformities of the flow due to the mesh were created downstream of the mesh and relaxed to roughly a homogeneous state of 9 % turbulence intensity in each direction at 100 mm downstream of the honeycomb ($v_w \cong 4.0$ m/s). The obstacles were placed at this location, shown with black circles in Figs. 2 and 3, to study the effect of the turbulence and eventually droplet transport around the cylinders in this well-controlled turbulent environment. The velocity accelerated to $v_w \cong 5.0$ m/s around the side of the cylinders, and formed a recirculation region behind the cylinders ($v_w \cong -1.0$ m/s). The turbulence intensity increased behind the cylinder ($\tau_w \cong 20$ % in a banded region behind the obstacle). The flow also decelerated to a stagnation region at the centerline, at the upstream face of the cylinders.

The experimental measurements were used for input and validation of the Sandia general-purpose fire simulation code, VULCAN, to study spray transport around cluttered spaces. The code was used to simulate the flow around the largest of the cylinders considered in the experiments. The initial conditions of the calculation were chosen to best match the experiments by setting the mean streamwise velocity, turbulence kinetic energy, and its dissipation to values of 4.5 m/s, 0.304 m²/s² and 0.0212 m²/s³, respectively. Comparison of the computational model predictions

to the PIV measurements indicated that qualitatively the location and size of the recirculation zone for the largest cylinder case was well captured. Quantitative comparison indicated that the numerical results over-predicted the streamwise mean velocity by 20 % and under-predicted the RMS in streamwise velocity by 15 %. These differences indicated that the numerical predictions under estimated the extent of turbulent mixing behind the cylinder, and may be attributed to the use of the k- ϵ model that is known to perform poorly in highly recirculating flows.

Droplet Transport in the Homogeneous Turbulent Flow Field

In this phase of the project, liquid fire suppressants were injected into the characterized homogenous turbulent flow field, and the droplet transport processes were investigated under a variety of conditions, as well as the interaction of the spray with different obstacles. The experimental arrangement was oriented horizontally, in place of the aforementioned vertical orientation, because of the need by the NGP Project 6A/1 effort to estimate the ratio of liquid agent impinging on the obstacle and the amount of agent transported past the obstacle. Of interest was also to determine whether droplets rebound and/or shatter off of the cylinder surface. Liquid agents were considered because of the effectiveness of high boiling point liquids to extract heat from a flame zone. The cylinder was heated to study the effects of a heated surface on droplet vaporization and transport, as a droplet approached the heated surface. Also, experiments were carried out with a more complicated body centered cube. Measurements included PIV, phase Doppler interferometry (to obtain spatial and temporal profiles of the size and velocity distributions) and, as well as visualization of the flow field. Measurements in the spray and flow field were carried out upstream and downstream of the obstacles.

To explore droplet transport around obstacles in a well-characterized homogeneous turbulent flow field, the experimental arrangement was modified, as shown in Fig. 4. The experiment was oriented horizontally to enable collection of liquid agent that dripped off of the obstacle, and prevented liquid droplets downstream of the obstacle from falling back upstream into the oncoming stream. The agent was water and was supplied to the flow field with a 60° hollow-cone pressure-jet atomizer. An octagon-shaped Plexiglas chamber, the front face that supported the inlet passages for the liquid agent and air, and back face that supported the exhaust passage, served to form a closed system with defined boundaries. A honeycomb layer was used to straighten the airflow, which was co-positioned around an injector for the agent. Grid-generated turbulence was imposed on the air stream by placing a square layer of wire mesh screen downstream of the honeycomb. For these experiments, the incoming air was directed entirely through a distributor plate with steel wool, circular cross-sectional area of the honeycomb, and then through wire mesh screen (placed 25 mm downstream of the honeycomb), as shown in Fig. 4. The face of the liquid atomizer was placed flush with the upstream side of the grid, and centered within one mesh cell so that the liquid spray would be unimpeded by the grid. The stepper-motor-driven traversing system translated the entire assembly, and permitted measurements of the flow field properties at selected locations downstream of the injector.

Measurements were carried out with two obstacles, an aluminum cylinder and a body-centered cube (BCC) arrangement of wooden spheres and connecting posts (see Figs. 5 and 6, respectively). The cylinder had a diameter

of 32 mm (305 mm in length), which was chosen because its diameter is larger than the integral length scale of turbulence. A hole was bored through the center for placement of a 250 W cartridge heater. The rod was also cut into two halves and 1 mm deep channels bored along one segment for placement of five K-type thermocouples. The thermocouples had an inconel sheath, ungrounded, and 0.8 mm in diameter (305 mm long). The thermocouples were placed in a cross pattern in the center of the rod (each separated by a distance along the surface of 6.4 mm, with the thermocouple junctions placed about 3.2 mm of the surface with bored holes at each location). The central thermocouple was used for temperature control of the heater, which was positioned behind the thermocouples. The BCC was composed of nine wooden spheres with a nominal diameter of 28 mm, all interconnected with posts, as shown in Fig. 6. The blockage ratio, or obstructed cross-sectional area for an equivalent area encompassing a face of the BCC, was about 64 %. The obstacles were placed nominally 182 mm downstream of the honeycomb, and centered with the atomizer centerline.

Particle image velocimetry measurements were carried out in the droplet-laden, homogeneous turbulent flow over both the unheated and heated cylinder, and body-centered cube arrangement of spheres. Transport of both water droplets and seed particles was characterized upstream and downstream of these obstacles. Data were recorded for the cylinder at ambient temperature and after being heated to 423 K to estimate the effects of the hot cylinder surface on droplet transport. The results indicated that smaller droplets were entrained into the recirculation region behind the cylinder while the larger droplets impacted the cylinder surface, accumulated and dripped off, and/or rebounded off the surface and dispersed radially outward into the free stream. The Weber number was too low to lead to droplet shattering. Significant spray cooling of the surface was observed for the heated cylinder, in addition to the presence of a vapor stream downstream of the cylinder along the shear layer region between the recirculation zone and free stream. Surface cooling that resulted from spray impingement was around 50 % of the preset cylinder temperature. For the BCC (with a blockage ratio of about 64 %), there was both transport of droplets and seed particles around and through the BCC, as well as significantly more liquid accumulation and dripping than for the cylinder.

The droplet-laden flow field over each obstacle was recorded with a digital movie camera at 9 frames/s. Examples of the observed droplet/particle transport processes are shown in Fig. 7 for a) seeded only and b) droplet only flow over the unheated cylinder, and c) combined droplet and seeded flow over the BCC. The seed was entrained in the turbulent flow field (see Fig. 7A) and a relatively high concentration of particles was observed in the wake behind the cylinder. On the other hand, the droplets in the center of the spray were found to impinge on the surface of the cylinder while those droplets at larger radial positions were transported around or past the cylinder with an increased radial component of velocity (see Fig. 7B). Few droplets were observed behind the cylinder in its wake. Droplets that impinged and wetted the cylinder surface dripped off at a rate of approximately one drop every 5 s. The transport of droplets through the BCC (see Fig. 7C) was interesting in that both the spheres and connecting rods (that simulate cylinders) block the droplets, while the flow field traversing through the obstacle provided an unobstructed path for the entrained droplets. Dripping was observed from each sphere at a rate of approximately

1 droplet/s. If one assumes that droplets fall off each sphere at this rate, one can determine that this liquid represents approximately 4.5 % of the inlet water flow (assuming a dripped droplet diameter of 8.5 mm, which was an estimated largest droplet size observed from digital movies). Although the BCC had more dripping of liquid than the cylinder, the major portion of the spray was still able to traverse the obstacle.

The above-mentioned laser sheet images indicated that dispersion of droplets/particles around the obstacle was dependent on its size. Comparison of the PIV velocity fields obtained with water droplets from the pressure-jet atomizer and 1 μm size seed particles formed from the fogging device also supported this finding. For example, the three components of droplet velocity for the flow over the unheated cylinder are presented in Fig. 8. In this figure, three cases are presented that represent the flow with the seed only, both seed and spray, and spray only. The black circle represents the position and size of the cylinder. The black contours lines represent stream traces (i.e., direction) of the in-plane velocity vectors. Comparison of the two cases with spray to the seed-only case indicated that the recirculation zone was somewhat larger for the spray cases. Larger size droplets required a longer distance to interact with the turbulent flow field, reduce their higher momentum, and be entrained into the recirculation zone, if at all. The stream trace (contour lines) also showed an unexpected pattern behind the cylinder near the stagnation point. Instead of presenting closed loops that indicate a time-integrated recirculating pattern, the contours appear to emanate from the stagnation region. One possible explanation is that there is a strong spanwise flow along the length of the cylinder. It appeared to be generated by the cylinder and may be related to the finite cylinder length (with an aspect ratio of about 10:1). Figure 9 presents the velocity field around the BCC for the combined spray/seed case. Although the configuration was more complicated, there were still similar features to the cylinder case. The flow accelerated around the spheres and there was reverse flow in the wake region. In addition, the presence of a cross-stream component of the flow was evident around the spheres. This cross flow may be a result of the three-dimensional nature of the spheres and flow field, and the transport of entrained droplets and aerosol particles through convoluted pathways of this obstacle.

Droplet Size and Velocity Distributions

The aforementioned results indicated that droplet surface impact, vaporization, and transport behind the cylinder were dependent on droplet size. Thus, this work focused on measurement of spatially and temporally resolved droplet size and velocity distributions in the upstream and downstream vicinity of the cylinder, using phase Doppler interferometry (PDI). Water was used as the liquid agent, with two additional agents, 3MTM fire protection fluorocarbons HFE-7100 (with a boiling point of 334 K) and HFE-7000 (with a boiling point of 307 K). Several strategies may be used to detect size dependent effects in regions where droplets rebound or vaporize. For example, a droplet near the upstream surface of the cylinder with a negative streamwise velocity (i.e., a droplet transported against the flow) would be indicative of a droplet rebounding off of the cylinder surface, and thus PDI would be used to obtain the associated droplet size. If the size distribution near the heated cylinder surface is devoid of relatively smaller size droplets, as compared to other locations away from the cylinder, then this result may be indicative of the effects of vaporization. These strategies were used in interpretation of the measurements.

Phase Doppler techniques involve creating an interference pattern in the region where two laser beams intersect, and results in a region consisting of alternating light and dark fringes. The region where the laser beams intersect is called the probe volume or sample volume. Due to the interference pattern, a droplet passing through the probe volume scatters light that exhibits an angular intensity distribution, which is characteristic of the size, refractive index, and velocity of the droplet. For a droplet with known refractive index, the size and velocity can be determined by analyzing the scattered light collected with several photomultiplier tubes. The PDI is a single-point (or spatially resolved) diagnostic instrument in that it obtains information about the spray at a single point in space. The PDI is also a single-particle instrument in that information is obtained for only one droplet at a time. This offers advantages over integrating techniques because the characteristics of a particular droplet (size, velocity, etc.) can be recorded and the data can be separated into classes (size classes, velocity classes) to further characterize the spray system.

The experiments were conducted using a two-component phase Doppler interferometer with a Real-time Signal Analyzer (RSA) available from TSI, Inc. A 5 W argon ion laser, operating in multi-line mode, was used as the illumination source. The blue (wavelength = 488 nm) and green (wavelength = 514.5 nm) lines of the argon ion laser were separated by beam conditioning optics, and focused by the transmitting optics to intersect and form the probe volume. The transmitting optics were coupled to the beam conditioning optics, using fiber optic cables to permit the transmitter to be located near the experiment. The front lens on the transmitter had a focal length of 500 mm. The green and blue beams had a beam separation distance of 39.9 mm and 40.2 mm, fringe spacing of 6.45 mm and 6.07 mm, and beam waist of 164 mm and 155 mm, respectively. Frequency shifting was set at 40 MHz. The receiver was located at a scattering angle of 30° measured from the direction of propagation of the laser beams. To accommodate the horizontal orientation of the experimental apparatus, the transmitter and receiver were positioned in a vertical plane, as shown in Fig. 10. Due to the large size of the receiver, the transmitter was positioned with the laser beams angled at 30° to the cylinder, which required correction of the cross-stream velocity. The front lens on the receiver had a focal length of 1000 mm. The spacing for the three PMT detectors (A, B, and C) that were used to carry out the sizing measurements was 34.8 mm for detectors A and B, and 101 mm for detectors A and C. A 150 mm slit aperture was located within the receiver to limit the length of the probe volume.

The measurements were carried out at several radial (R, cross-stream) positions and over a range of axial (Z, streamwise) positions upstream and downstream of the cylinder. Figure 11 illustrates the measurement grid that was used and the location of the cylinder relative to the grid mesh. Measurements were carried out from approximately 50 mm upstream of the cylinder to a downstream position of 100 mm. An increment of 2.5 mm was used for $-25.4 \text{ mm} < Z < 38.1 \text{ mm}$, and an increment of 12.7 mm for all other axial positions. In the radial direction, measurements were carried out in increments of 5 mm from 0 to 20 mm in the upper hemisphere (i.e., in the positive radial direction). Data were not obtained immediately downstream of the cylinder (i.e., for $\approx 25 \text{ mm} < Z < 14.6 \text{ mm}$) because the signals were too low to detect any droplets.

As report earlier, the droplet-laden flow field over both the unheated and heated obstacle was recorded with a high-resolution digital camera (providing both still-images and movies at 9 frames/s). Droplets were observed in the center of the spray impinging on the surface of the cylinder and dripping off at the bottom of the cylinder, while those droplets at larger radial positions were transported around the cylinder. Movies obtained with a high-speed digital camera at 1000 frames per second indicated that many impinging droplets rebounded off of the surface and into the free stream. More rebounding droplets were observed when the air velocity was zero. Few larger size droplets were observed behind the cylinder in its wake, but were abundant with the smaller size aerosol seed that were introduced to the flow through the air stream. There was no evidence of secondary breakup of the droplets, which was expected because the Weber number was much smaller than the critical value for droplet shattering.

When the cylinder was heated to 423 K (i.e., well above the boiling point of water), the droplet-laden flow over the cylinder appeared to be similar to the unheated case except along the shear layer downstream of the cylinder. In this region, as mentioned earlier, a vapor layer formed which was presumed to be the result of vaporization of the liquid that wets the hot surface. It was expected that vaporization of liquid near the cylinder surface may influence locally the transport of droplets behind the cylinder by vaporizing the smaller size droplets, and thus was a focus of this segment of the investigation.

A solid-cone nozzle was used to increase the number of droplets impinging on the cylinder surface (a hollow-cone atomizer was used earlier with PIV measurements). It was observed that drippings off the cylinder occurred at a rate of approximately 6.5 mL/min for the unheated cylinder, while there was no dripping for the heated cylinder due to droplet vaporization. It was also observed by the PDI laser beam intensity that the concentration of droplets behind the cylinder was significantly reduced. For the heated cylinder, the cylinder surface temperature varied significantly with time after the spray was introduced to the flow field. However, it is unknown at this time whether these changes are attributable to time-varying changes in the response time of the cylinder heater during droplet impingement, or to some other systemic issue.

The PDI was used to provide information on: 1) droplets rebounding off the upstream face of the cylinder, 2) vaporization of droplets near the heated cylinder, 3) droplet sizes entrained into the recirculation region behind the cylinder, and 4) the effect of agent boiling point on droplet transport. The unheated cylinder results for the Sauter mean diameter (D_{32}) and droplet mean streamwise component of velocity (U) are presented in Fig. 12. The rectangle located on the abscissa at an axial position of $Z \cong \pm 14.6$ mm represents the location of the cylinder. The gap in the data for the radial positions $R = 0, 5$ mm, and 10 mm indicates the presence of the cylinder. For Fig. 12A, the general trends were: 1) a decrease in mean size on the downstream side of the cylinder, as compared to the upstream side, and 2) an increase in mean size with increasing radial distance from the central plane of the cylinder. The latter was indicative of the presence of more smaller size droplets near the center of the spray, as exemplified by the results obtained at the upstream axial position of $Z = -50$ mm, which was attributed to the design characteristics of the atomizer. For the droplet mean streamwise velocity (see Fig. 12B), the values increased with decreasing

radial position at the upstream position of $Z = -50$ mm. These higher velocities correlate with the smaller droplet mean size near the center of the spray. As droplets approach the upstream surface of the cylinder, there is a decrease in the streamwise velocity component and an increase in the cross-stream component. There is an increase in the droplet streamwise velocity over the cylinder for $R = 15$ mm, and 20 mm, which is also characteristic of the accelerated flow over the cylinder, as described earlier. At locations near the upstream surface of the cylinder, negative values for the streamwise velocity are detected (see Fig. 13), which may be indicative of droplets rebounding off of the surface. However, positive values of velocity are obtained for the abundance of droplets, which indicates that these impinging droplets either adhere to the cylinder surface or rebound at an angle that maintains their momentum in the downstream direction over the cylinder. Note that the symbols in Fig. 13 are sized according to the actual droplet diameter.

The droplet streamwise velocities decrease and become negative values for $R = 0, 5$ mm, and 10 mm on the downstream side of the cylinder, which is indicative of the presence of a recirculation zone and the entrainment of these droplets into this zone. Although the magnitude of the droplet mean streamwise velocity downstream of the cylinder is negative, indicating the presence of a recirculation region, it is clear that the mean is representative of a distribution of velocities and associated droplet sizes. This point is highlighted in Fig. 14, which presents the droplet streamwise velocity with respect to droplet interarrival time into the probe volume at two points downstream of the cylinder within the recirculation region. One measurement location along the centerline, at $Z = 25$ mm (see Fig. 14A), represents a measurement close to the cylinder, while the other, at $Z = 76$ mm (see Fig. 14B), represents a location near the downstream edge of the recirculation pattern. The results for $Z = 25$ mm indicate that many droplets are recirculated upstream toward the cylinder (because $U < 0$), as expected, but also indicate that several droplets at this location are transported in the downstream direction (i.e., $U > 0$). One can speculate that these latter droplets either originate in the recirculation zone or are transported around the cylinder surface and penetrate directly into the recirculation region. In addition, the droplet size does not provide additional information since the size for these droplets varies between $5 \mu\text{m}$ and $30 \mu\text{m}$, and this range is similar to that for the size distribution for the entire population for this measurement. In a similar vane, the results in Fig. 14B indicate that the abundance of droplets are transported in the downstream direction at this point (i.e., for $U > 0$). However, a few droplets are entrained into the recirculation region (i.e., for $U < 0$).

Comparison of results for the unheated and heated cylinders indicates consistently that the value of D_{32} are smaller for the heated case as the droplets are transported past the cylinder surface. The droplet streamwise and cross-stream components of velocity are also lower for the heated case. The unheated and heated results are compared in Fig. 15 for D_{32} and U at $R = 20$ mm. The decrease in the values of both D_{32} and U for the heated case indicates that droplet vaporization does not result in the complete removal of the smaller size droplets from the distribution, but instead a decrease in the size of all droplets (which results in an overall decrease in both the mean size and velocity). In fact, the droplet size distributions illustrate clearly the shift of the entire distribution to smaller sizes for the heated cylinder.

Droplets with lower boiling points (i.e., the HFE agents as compared to water) were observed to vaporize more readily, resulting in vaporization of droplets before reaching the obstacle, and the absence of dripping off the cylinder surface. Comparison of results for the three agents indicates that droplet size increases and velocity decreases with increasing agent boiling point. Figure 16 presents a comparison of the droplet mean size and streamwise velocity with streamwise position for the three agents at $R = 20$ mm. The size distribution for each agent is also found to shift to larger sizes for increasing agent boiling point.

RECOMMENDATIONS FOR FUTURE RESEARCH:

Of paramount importance for validation of computational models is to provide a database with specified experimental uncertainties so that the modeler will have the highest confidence in using the data. To achieve such a database requires inlet and boundary conditions, and experimental measurements to be repeated several times to determine uncertainty levels. In addition, as the Vulcan fire code continues to be developed, data will be required to address specific issues that arise regarding the actual physics and modeling of the subgrid. This study presented some information on the effect of agent boiling point; however, it would be more efficacious to carry out a parametric investigation of different agent physical properties on droplet transport processes. Additional information regarding atomizer design, spray pattern, droplet spatial variation containing specified droplet sizes, more complicated obstacle arrangements, and droplet composition (e.g., droplets with other effective suppressants such as in miscible solution or colloidal suspensions) may provide important information for the modeling effort. Also, simulating different scenarios of fire suppression, such as by putting tail tale heaters behind obstacles and introducing the liquid agent suppressant, are important in confirming the efficacy of various effects, like droplet size, velocity, composition, and spatial density, on reaching and extinguishing a fire.

CONCLUSIONS:

During the three years of this project, a startup data set was developed to guide the modeling efforts under the NGP project "Fire Suppressant Dynamics in Cluttered DoD Weapon System Compartments (6A/1)". The collaborative effort worked well, in which our experiments were coordinated by the fruitful and frequent discussions with the NGP 6A/1 participants (Sandia Nat'l Labs, NavAir, and the USAF 46th Test Wing), and resulted in a data set that was responsive to the modeling needs. Particle image velocimetry measurements and numerical predictions were compared for a turbulent flow over cylindrical obstacles. Comparisons of the flow field computational predictions by Sandia to the experimental results obtained in this study showed reasonable agreement. A numerical sensitivity study of initial droplet size revealed that droplet penetration around obstacles is dependent on droplet size. Particle image velocimetry measurements were carried out for a droplet-laden, homogeneous turbulent flow over an unheated and heated cylinder, and body-centered cube arrangement of spheres. Droplets were observed to impact the cylinder surface and either wet (leading to dripping) or rebound off the surface. Significant spray cooling of the surface and the presence of a vapor stream downstream of the cylinder along the shear layer was observed for the heated cylinder. Comparison of the velocity fields obtained with water droplets from a pressure-jet atomizer and

1 μm size aerosol particles, formed from a fogging device, indicated that dispersion of droplets/particles around an obstacle was dependent on its size.

Phase Doppler measurements were carried out to obtain droplet size and velocity distributions in a droplet-laden homogenous turbulent flow field around a cylindrical obstacle. Results indicated that most impinging droplets coat the surface with few droplets rebounding back into the free stream. Rebounding droplets were generally less than 30 μm , corresponding to the higher probability portion of the size distribution. Downstream in the wake region of the cylinder, a distribution of smaller size droplets (generally, of less than 30 μm) was entrained into the recirculation zone. Droplets larger than 30 μm were found to impinge on the cylinder surface or disperse around the cylinder to be transported far downstream of the obstacle. Near the heated cylinder surface, droplet vaporization resulted in smaller mean droplet sizes, as compared to the ambient case. Droplets with lower boiling points were found to vaporize more readily, resulting in vaporization of droplets before reaching the obstacle, and the absence of dripping off the cylinder surface. Droplet size and velocity decreased with increased cylinder temperature. Droplet size increased and velocity decreased with increasing agent boiling point. It is improbable that droplet shattering occurred for the Weber numbers (i.e., droplet sizes and velocities) encountered for the given operating conditions (typical of that in engine nacelles).

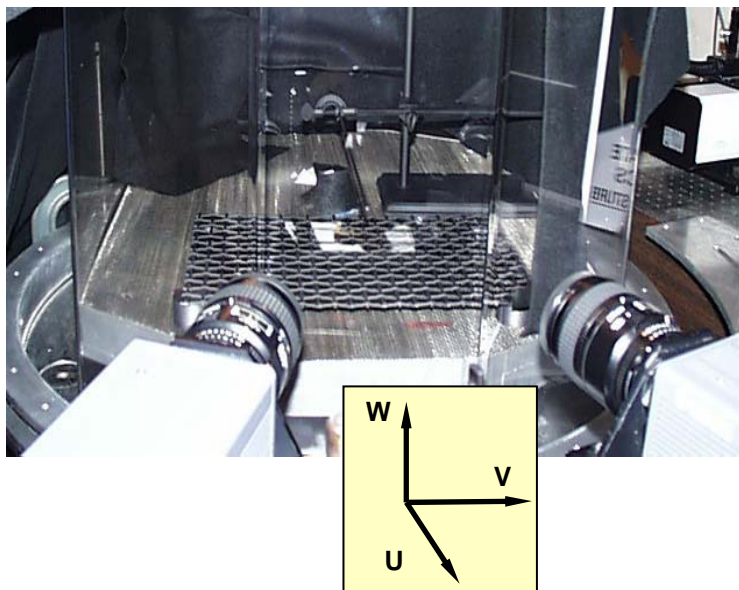
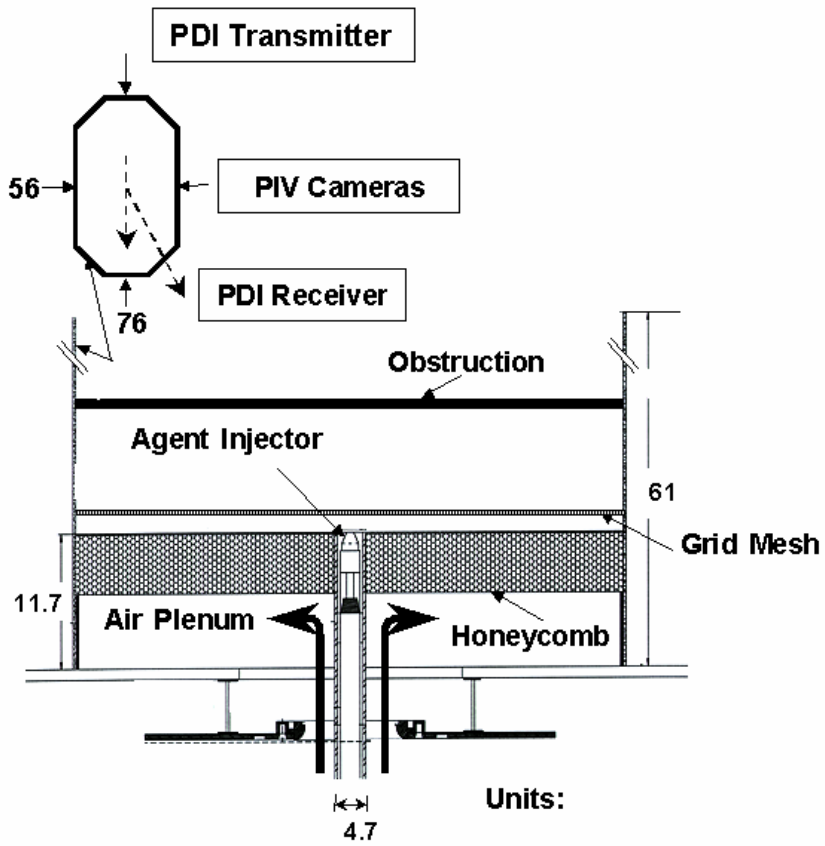


Figure 1: View of the initial experimental arrangement with cameras from the PIV system in the foreground.

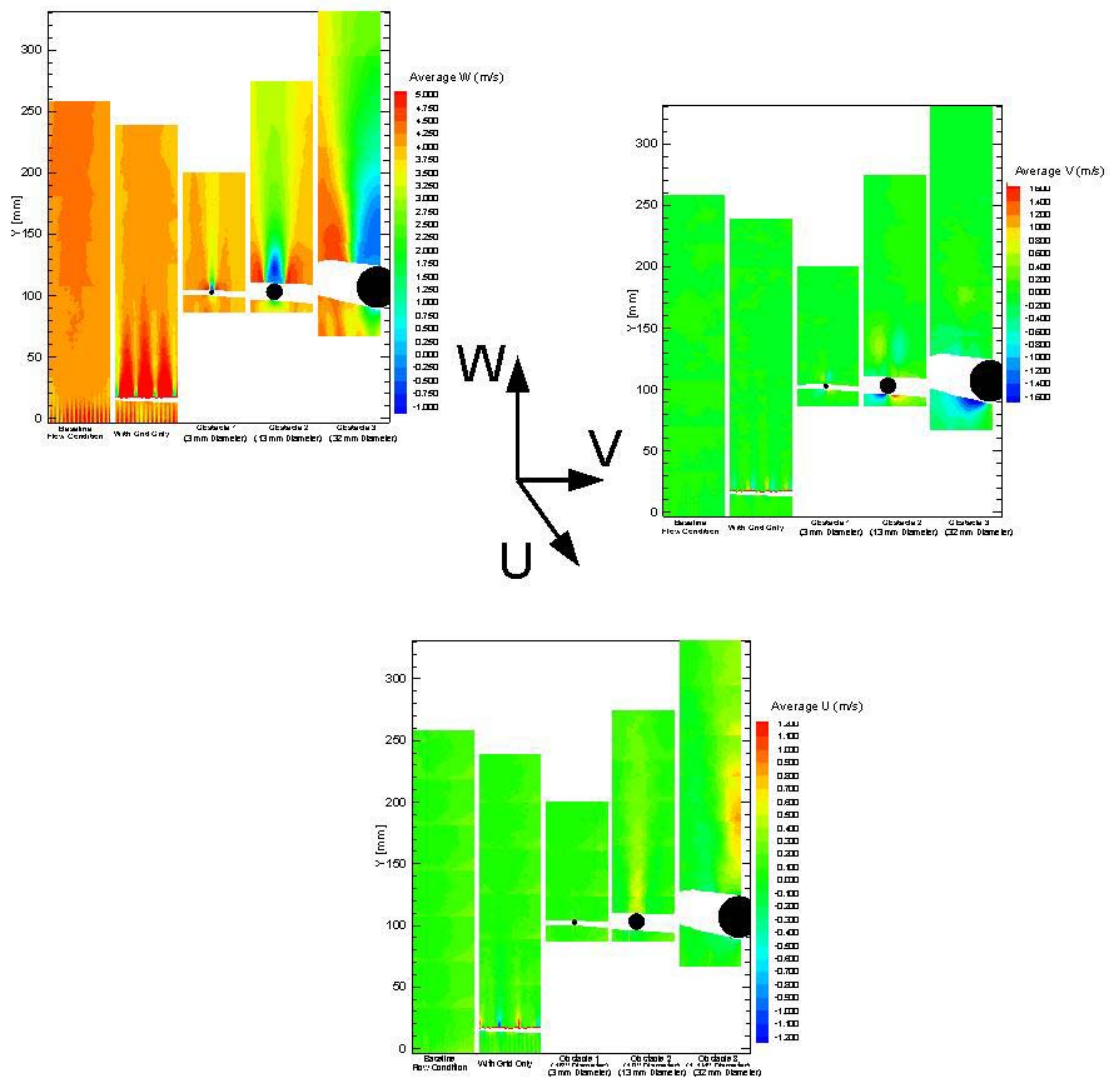


Figure 2: Variation of mean streamwise and cross-stream velocities with downstream distance.

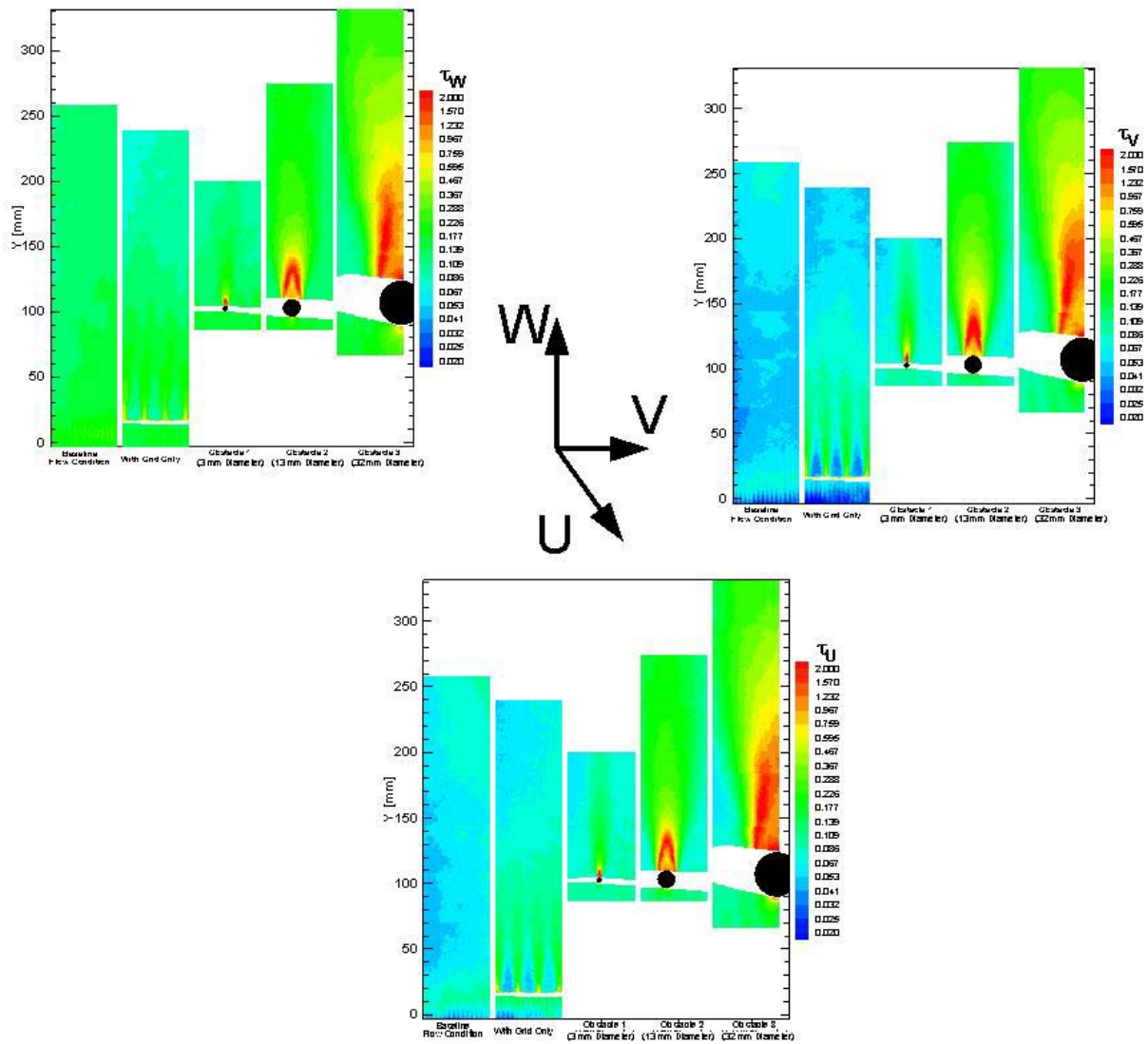


Figure 3: Variation of mean streamwise and cross-stream turbulence intensities with downstream distance.

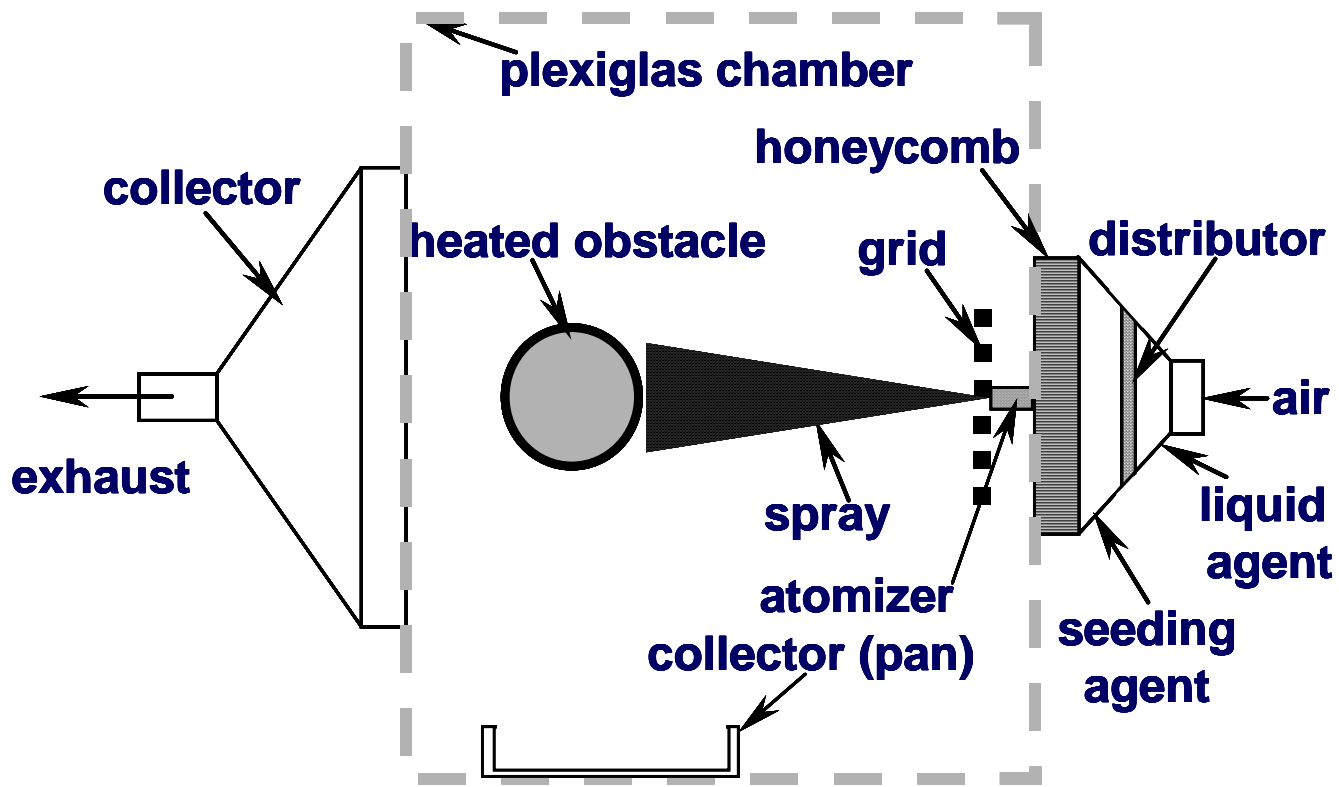
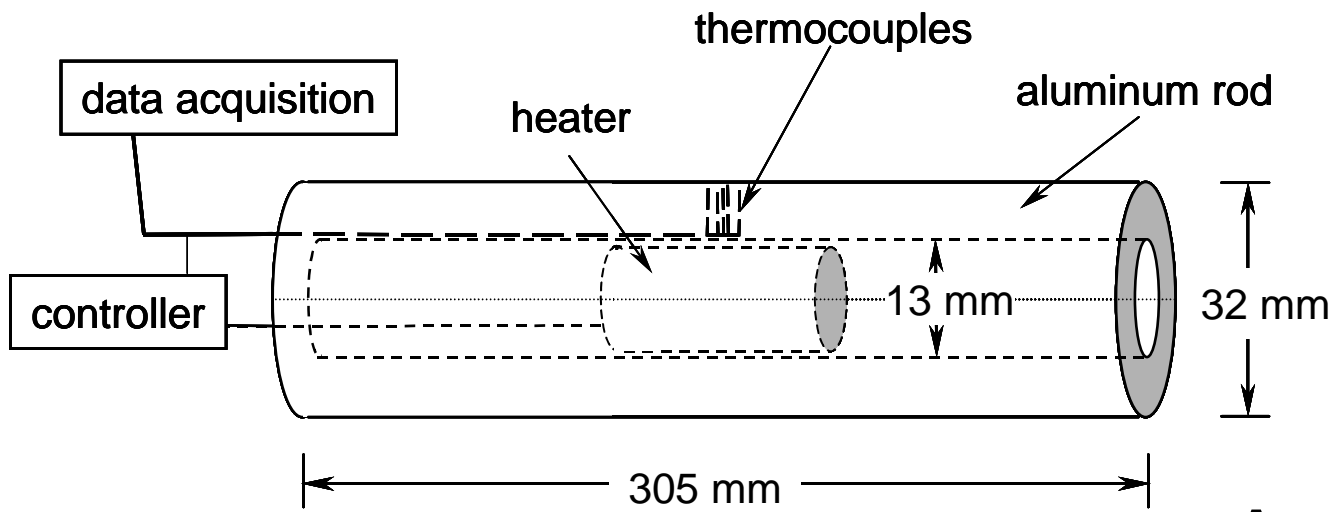
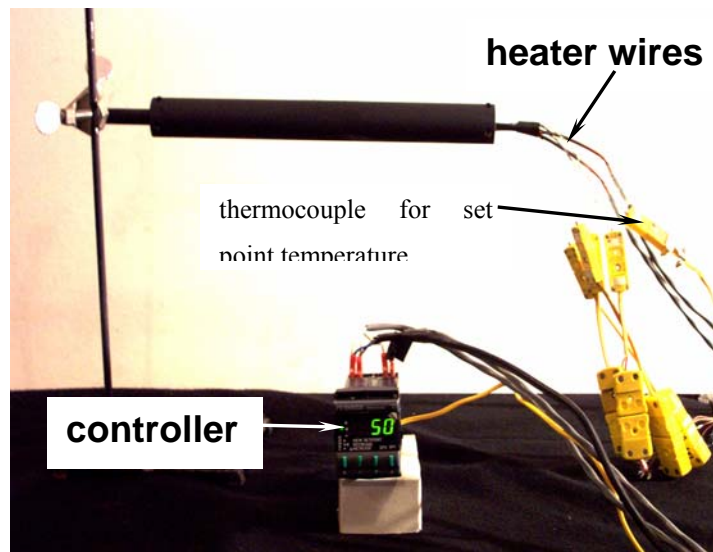


Figure 4. Schematic of the experimental arrangement for the droplet laden grid-generated turbulent flow field.



A



B

Figure 5. Experimental arrangement for the heated cylinder: A) schematic and B) front view.

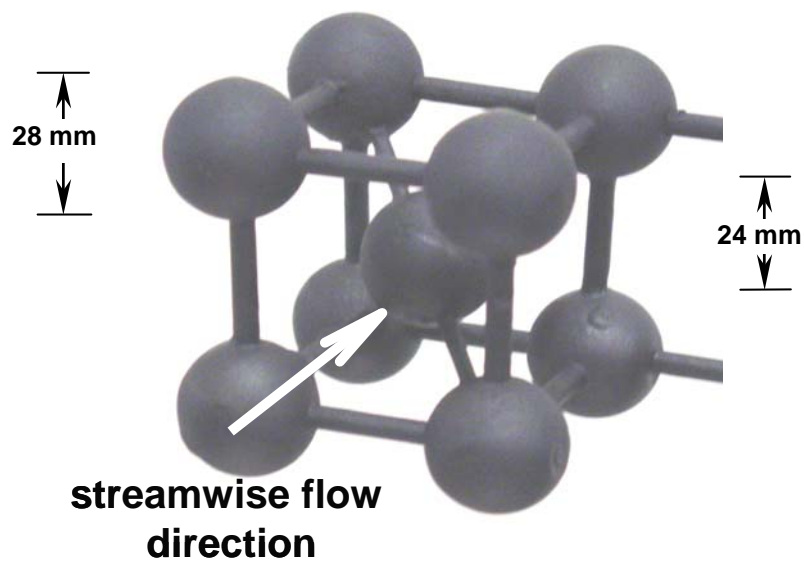
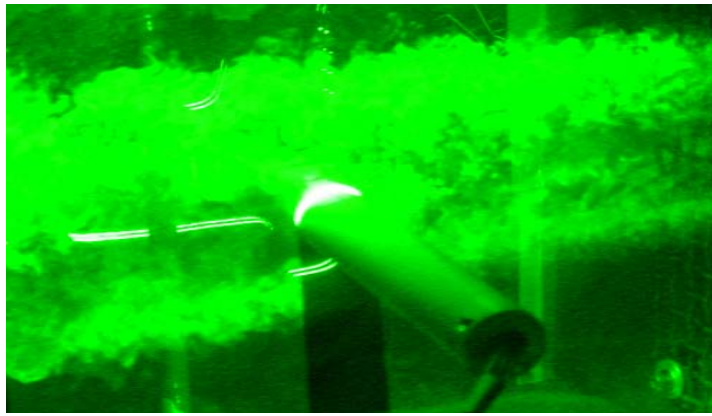


Figure 6. View of the body-centered cube of spheres.



A



B



C

Figure 7. Photographs of the A) seed/droplet-laden flow field around the unheated cylinder, B) droplet-laden flow field around the unheated cylinder, and C) seed/droplet-laden flow field around the body-centered cube of spheres. Flow direction is from right to left.

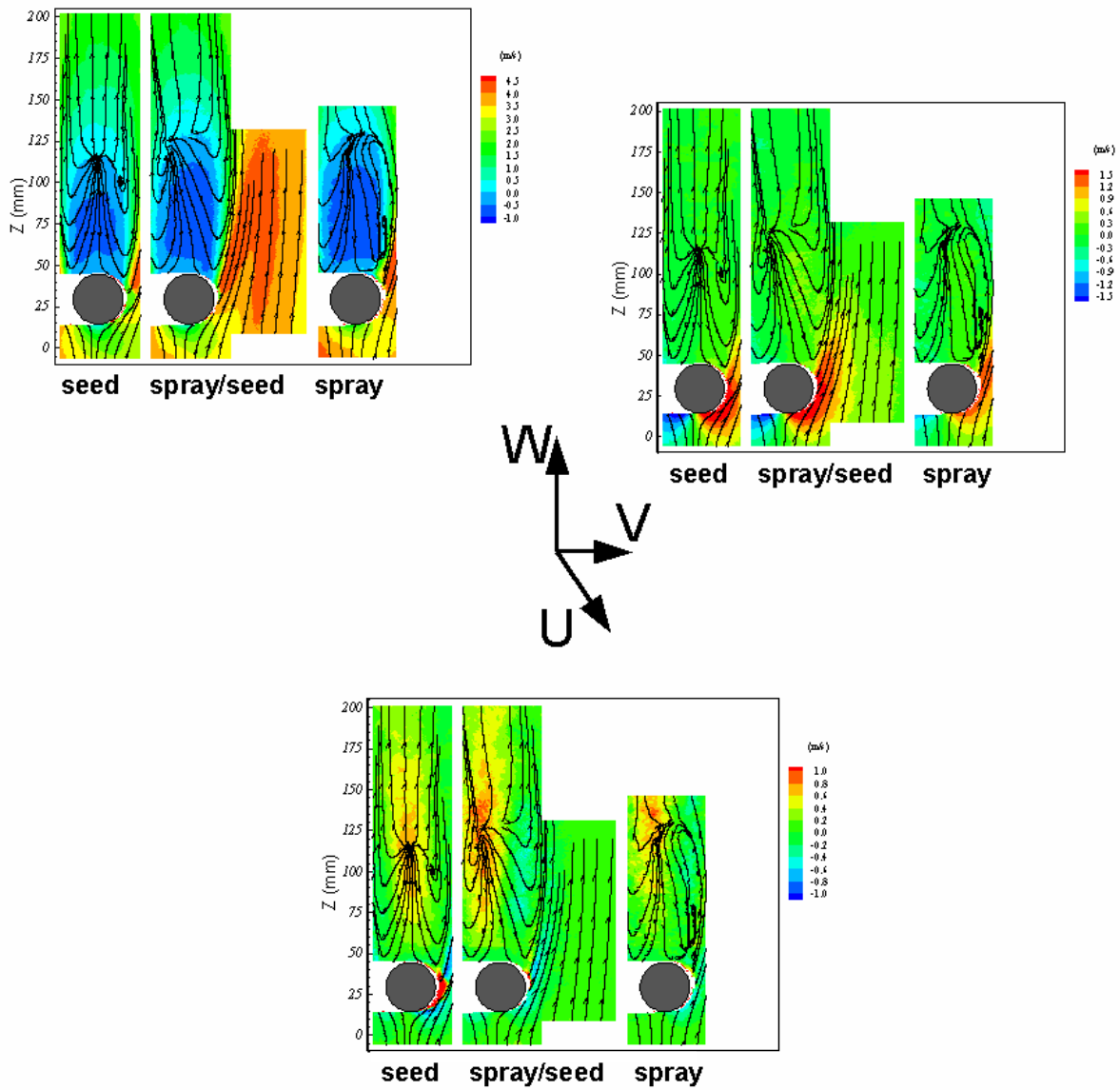


Figure 8. Variation of the mean streamwise and cross-stream velocities with downstream distance for the unheated cylinder. Contours are the stream traces of the in-plane vectors obtained from the axial and radial components of velocity.

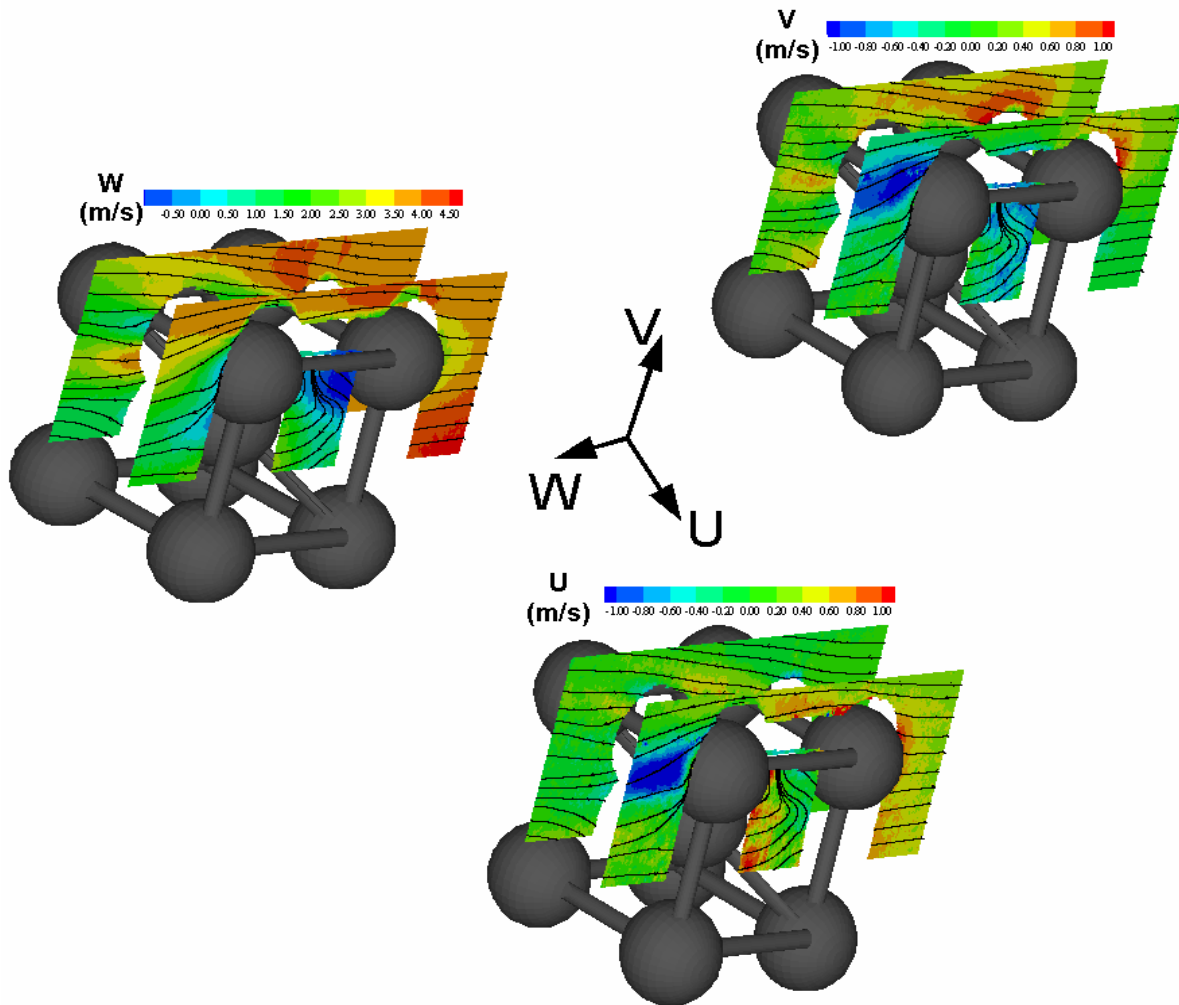


Figure 9. Variation of the mean streamwise and cross-stream velocities with downstream distance for the body-centered cube of spheres. Contours are the stream traces of the in-plane vectors obtained from the axial and radial components of velocity.

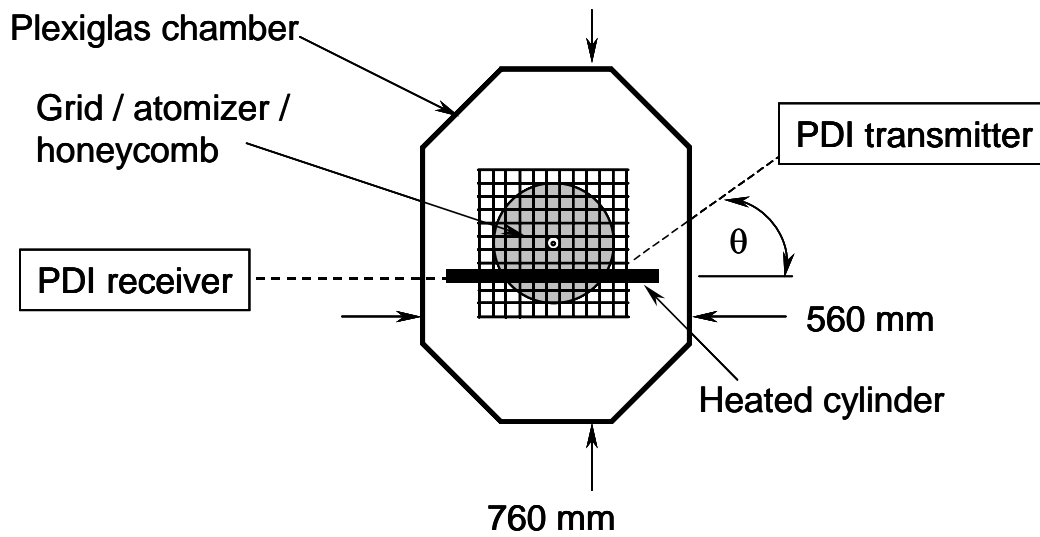
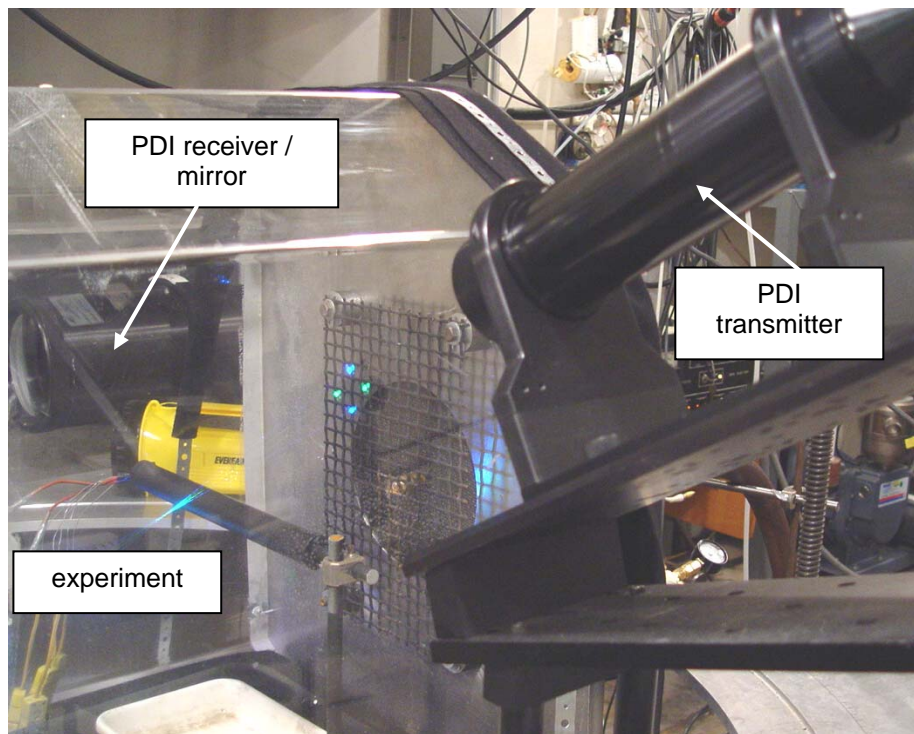


Figure 10. View and schematic of the experimental arrangement with the laser from the phase Doppler interferometry system.

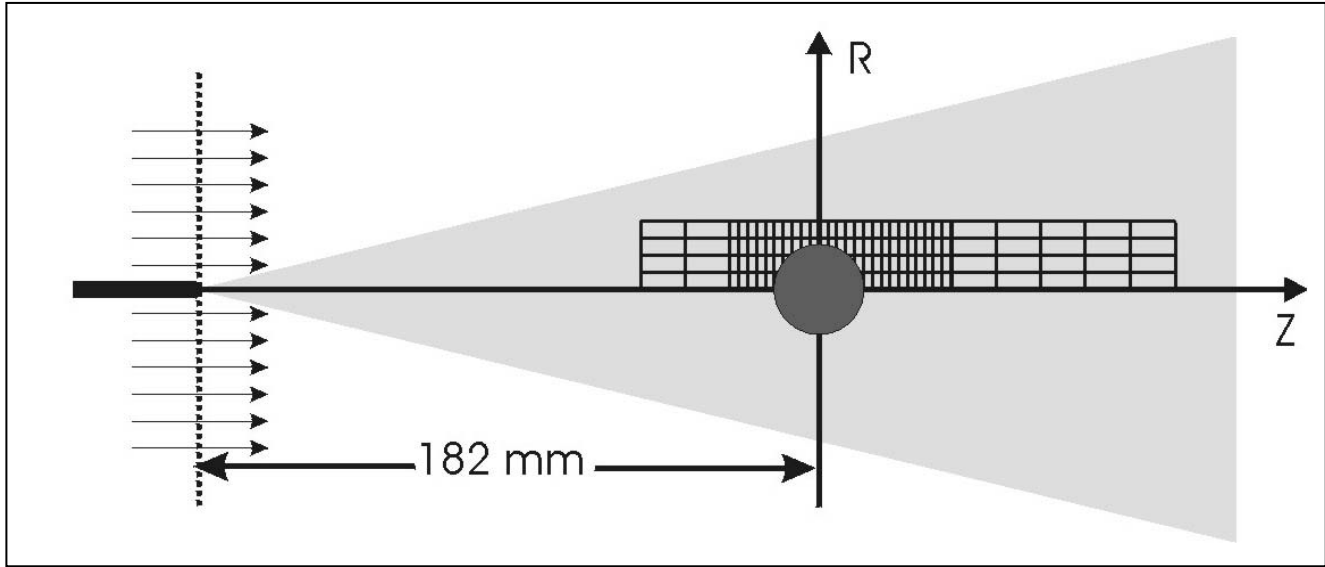


Figure 11. Schematic of the measurement grid around the cylinder.

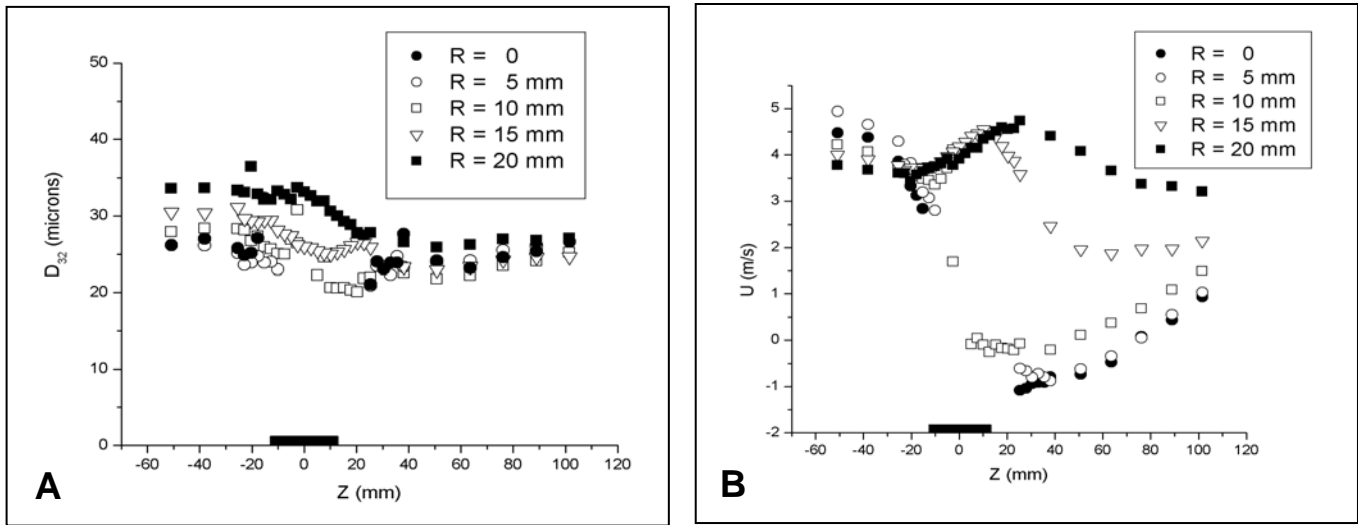


Figure 12. Variation of droplet A) Sauter mean diameter and B) mean streamwise velocity with streamwise position at different cross-stream positions for the unheated cylinder.

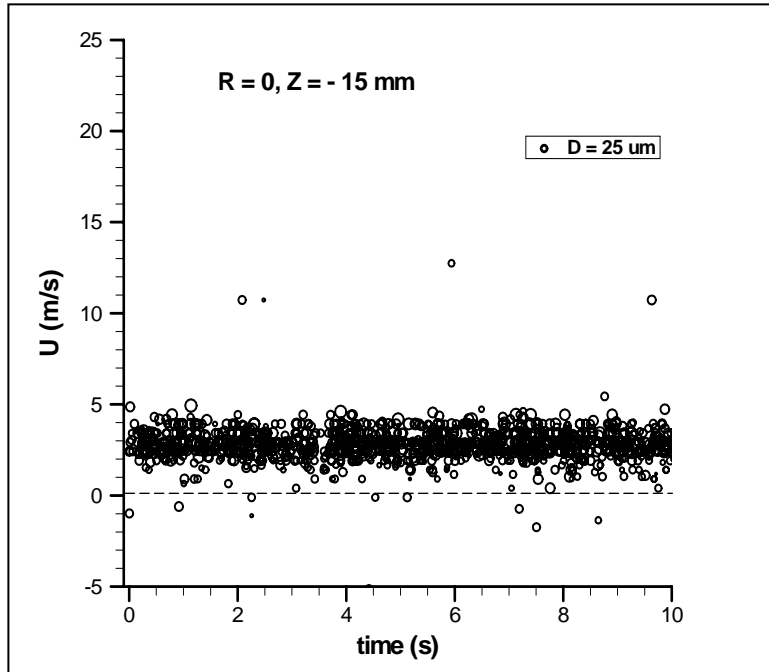


Figure 13. Variation of the streamwise velocity with time upstream of the unheated cylinder at $Z = -15 \text{ mm}$ and along the centerline.

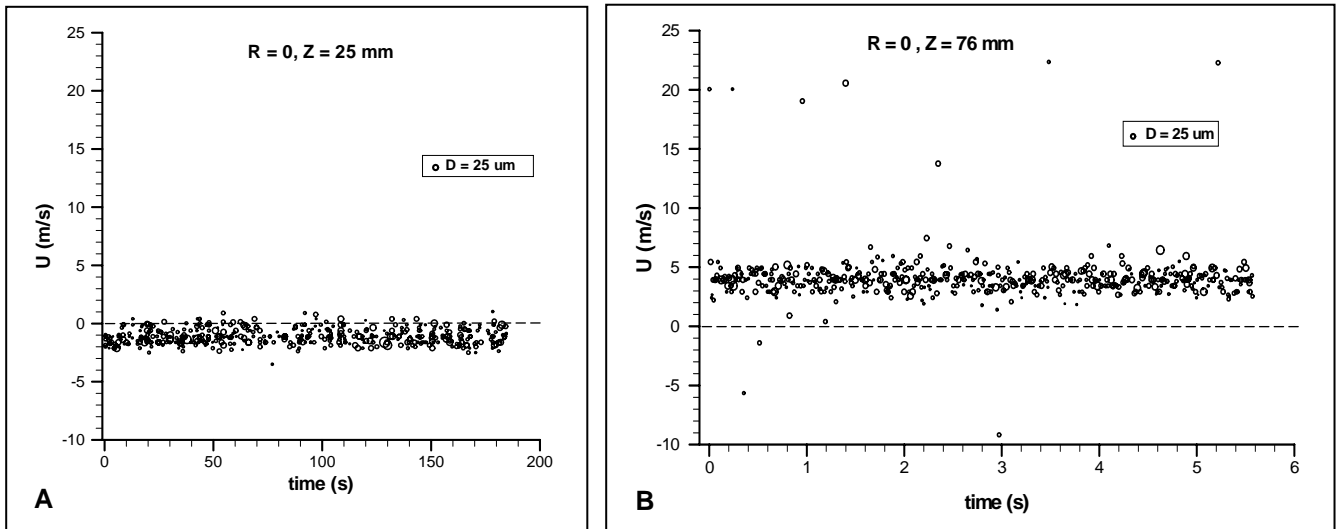


Figure 14. Variation of the streamwise velocity with time at two streamwise positions of A) $Z = 25 \text{ mm}$ and B) $Z = 76 \text{ mm}$ along the centerline, downstream of the unheated cylinder within the recirculation region.

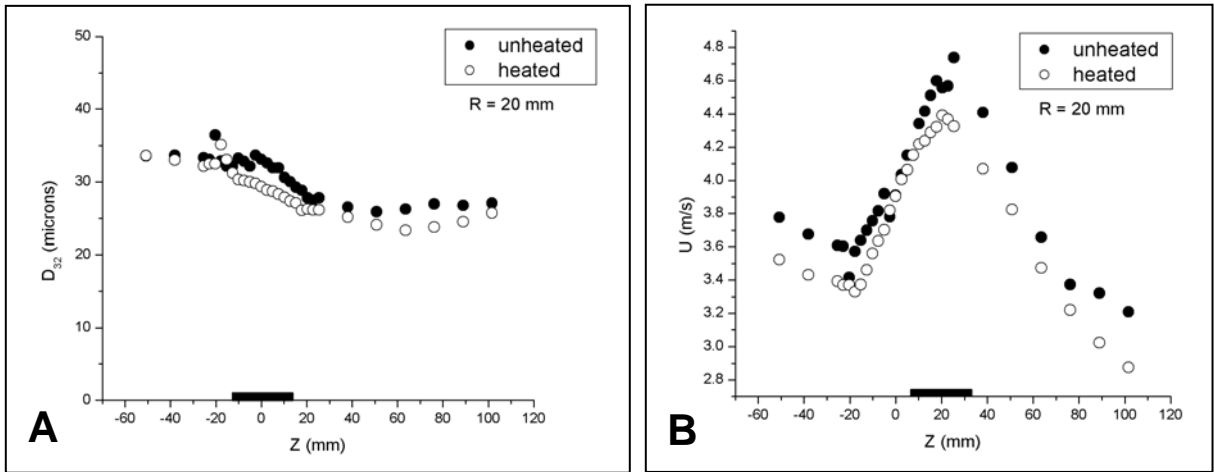


Figure 15. Variation of droplet A) Sauter mean diameter and B) mean streamwise velocity for the unheated and heated cylinders.

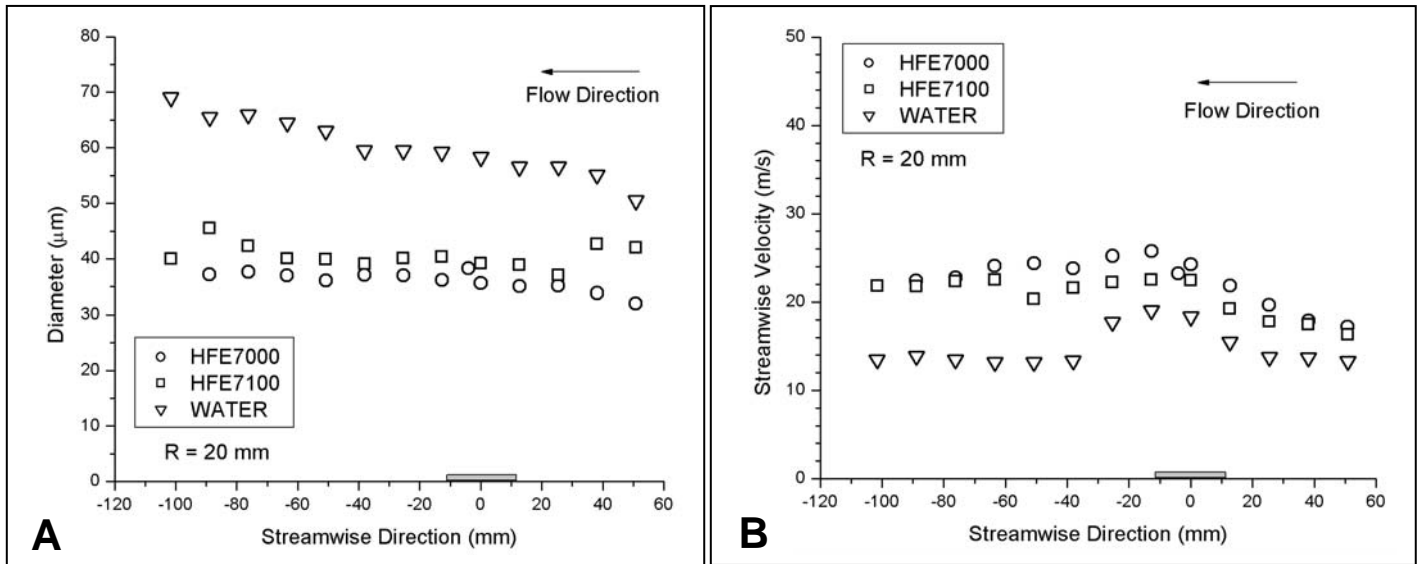


Figure 16. Comparison of the droplet A) mean size and B) streamwise velocity for the three agents.